JOURNAL OF GEOPHYSICAL RESEARCH, VOL. 95, NO. C2, PAGES 1599–1613, FEBRUARY 15, 1990

Variations in the Structure of the Anticyclonic Gyres Found in the Alboran Sea

GEORGE W. HEBURN AND PAUL E. LA VIOLETTE

Naval Oceanographic and Atmospheric Research Laboratory, Stennis Space Center, Mississippi

Historical satellite, aircraft, and in situ data have shown that two anticyclonic gyres (the western and eastern Alboran gyres) are major ocean features of the Alboran Sea. An examination of several years of satellite imagery indicates that large variations in the surface expression of these two gyres occur and that on occasion one or the other gyre disappears (the disappearance of both gyres at the same time was not seen). The initial disappearance of either gyre occurs on a time scale of a week to 2 weeks, whereas the return may take from 3 weeks to 2 months. Various forcing mechanisms, i.e., winds, mass flux inflow through the Straits of Gibraltar and Sicily, and/or density, have been used in numerical ocean circulation models to study the dynamics of the western Mediterranean Sea. Various model results show relationships similar to those shown by the satellite imagery. However, no single forcing mechanism has been positively identified as the source of the disappearances, and the events may be a result of a combination of forcing mechanisms.

INTRODUCTION

The Alboran Sea is an area of transition between the Atlantic Ocean and the Mediterranean Sea [e.g., *Lanoix*, 1974; *Lacombe and Tchernia*, 1972; *Gascard and Richez*, 1985; *Parilla et al.*, 1986]. The surface flow of water of Atlantic origin moving through the Alboran Sea enters from the Strait of Gibraltar and exits into the western Mediterranean proper. (Because of the strong changes in salinity that take place during this and subsequent movement of this surface layer, we call the water Modified Atlantic Water, or MAW.) This surface flow overrides a deeper layer of dense Mediterranean Water (MW) outpouring through the Alboran into the strait and then the Atlantic. The main inflow path of the MAW is around two anticyclonic gyres (the western and eastern Alboran gyres) that dominate the sea's circulation (Figure 1).

Lanoix [1974], using multiship data from campaigns conducted in July–August 1962, showed that MAW enters the northeastern Alboran via the Strait of Gibraltar as a strong jet (1.6 Sv). The inflowing jet initiates the western Alboran gyre in the basin west of Cape Tres Forcas. There the gyre sits, forming a large rotating bowl (200–300 m deep) of low-salinity MAW that gradually mixes with the more saline MW at depth. Model studies of the region [e.g., *Preller and Hurlburt*, 1982; *Heburn*, 1985*a*, 1987] indicate that the formation, mean position, and shape of the western gyre are controlled by several factors: the narrowness of the Strait of Gibraltar, the angle of the strait with respect to the Alboran Sea, the geometry of the Alboran Basin, and the effect of the Earth's rotation.

The most intensive investigations of the western Alboran gyre since the 1962 campaigns were made in 1982 during the Donde Va? multiplatform experiment [*Donde Va? Group*, 1984]. *Perkins et al.* [1989] used current meter mooring and satellite infrared data to show that the western gyre was not present for at least a 9-day period during the 5-month Donde Va? experiment. The studies show that during the period when the gyre was absent, the inflow adopted an abrupt southerly course after leaving the strait.

Field studies of the Alboran Sea that included the eastern Alboran gyre have been few [e.g., *Lanoix*, 1974; *Cheney*, 1978; *Cheney and Doblar*, 1982]. Whereas *Cheney*'s [1978] analysis of November 1976 and March 1977 data indicated the presence of an eastern gyre, a later study of October 1977 data did not appear to show a gyre. Early model studies of the Alboran Sea such as *Preller and Hurlburt*'s [1982] did not indicate a second gyre east of Cape Tres Forcas. The second gyre has been repeatedly seen in the satellite thermal imagery of the region [e.g., *Phillipe and Harang*, 1982]. However, the structures of both it and the western gyre are not always as clearly defined as the classic portrayal presented in Figure 1.

The Western Mediterranean Circulation Experiment (WMCE) [*La Violette*, 1987] conducted in situ studies specifically aimed at the eastern gyre in a winter campaign in 1986. *Tintore et al.*'s [1988] analysis of the data from this campaign concentrated on the eastern edge of the gyre. Their analyses, as well as preliminary studies of more recent campaigns by other investigators [e.g., *Arnone et al.*, 1987], have indicated the eastern Alboran gyre to be as complex as the western Alboran gyre.

In an examination of satellite imagery, the present authors noted that for periods of several weeks, one or the other of the two gyres did not appear. This absence of the eastern gyre may have occurred during the early field campaigns and may be the reason that the eastern gyre was not always detected (Figure 2). Indeed, as noted by *Perkins et al.* [1990], the western gyre disappeared only 4 weeks before the start of the intensive field phase of Donde Va? If that phase had started 1 month earlier, the data would not have shown the presence of a western gyre.

We present a study of satellite imagery to derive an approximation of the frequency and duration of the gyre disappearances. We then use numerical ocean circulation models to study the dynamics of the western Mediterranean Sea under the influence of various forcing mechanisms (e.g., winds, inflow/outflow mass transport through the straits, topography, and density changes due to surface fluxes of heat and salt). The model results will be used to illustrate

Paper number 89JC03578.

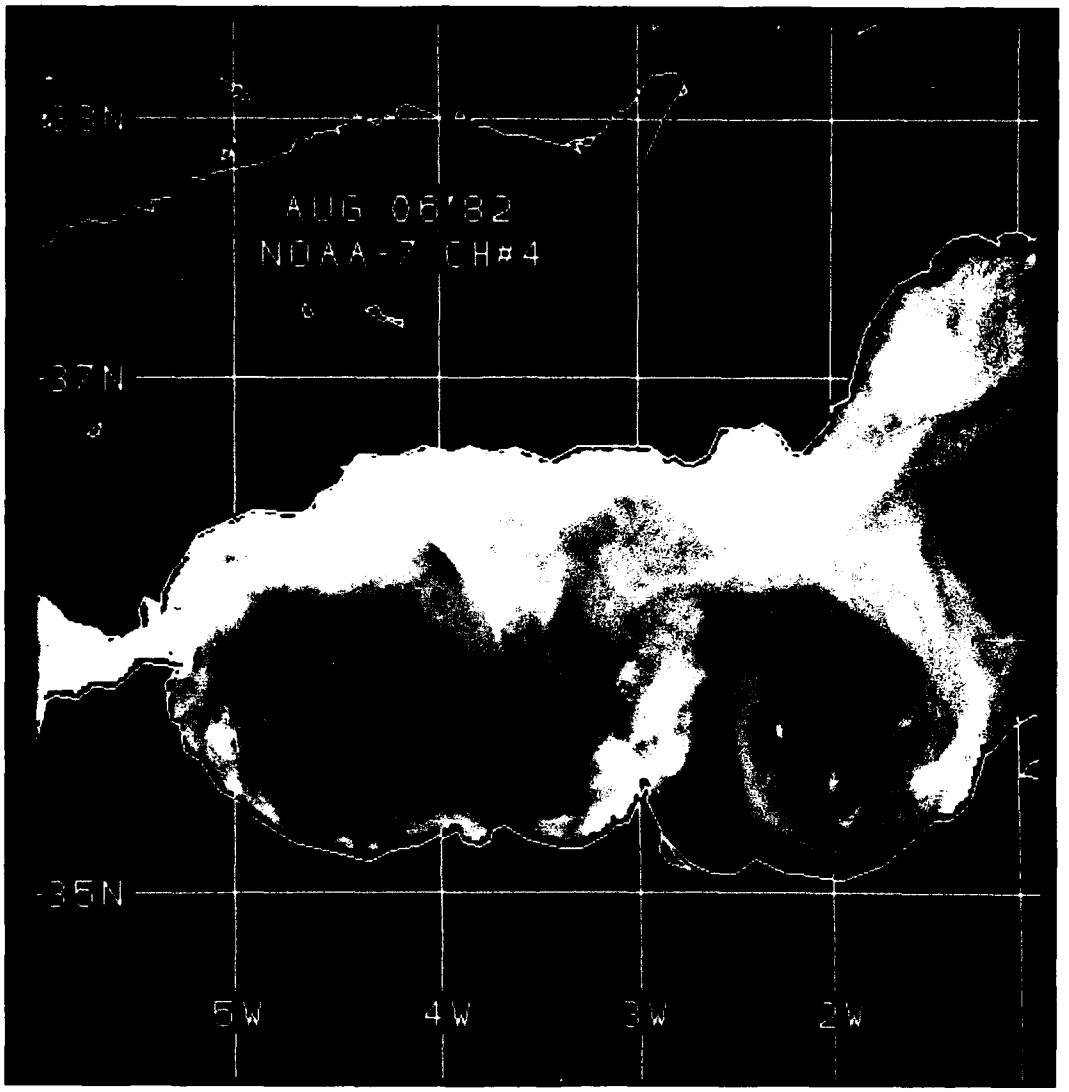

Fig. 1. A classical portrayal of the two Alboran Sea anticyclonic gyres as seen by the thermal sensor of the NOAA 7 satellite. This image and the other images presented in this study have not been atmospherically corrected. The darker tones in the images refer to warmer water, whereas the lighter tones refer to the colder water.

relationships similar to the satellite imagery and indicate possible causes/hypotheses for the variations in the paths of the two gyres which need further observational and theoretical investigation.

SATELLITE IMAGERY

Although changes in salinity dominate, the thermal fields displayed in satellite infrared imagery can be used as tracers of the flow [*La Violette*, 1984; *Arnone and La Violette*, 1986]. Most important for this study, they graphically display the disposition of the two gyres. The primary satellite sensor used in these studies is the advanced very high resolution radiometer (AVHRR) of the NOAA series (NOAA 7-10). Channel 4, operating in the electromagnetic thermal range of 10.3–11.3 microns, was used to provide uncorrected (i.e., for atmosphere) radiation temperatures.

There are problems in working with long-term thermal satellite data in the Alboran Sea, cloud cover being the most difficult, followed by seasonal change. Some seasons show poor thermal gradients (spring and fall), while others show reversals in the distribution of cold and warm water (winter and summer). For this study, however, the importance is not actual thermal values, but gross thermal patterns and the variation in the geographic distribution of these patterns.

The satellite images involved in this study cover the period 1977–1987. All together, 196 images were examined that showed the region of the gyres sufficiently cloud-free to define the presence or absence of either gyre. Most of the satellite data (146 images) are for the years of the Donde Va? (1982) and WMCE (1986) experiments (Table 1). As these data were the most continuous, they allowed a rough temporal sequence to be established. The remaining 50 images are of interest, in that they show that each of the gyres was not present during other years of the decade (this occurred in 20% of the images. However, these images are scattered in time to tell when any single disappearance occurred in the time between any of the 50 images.

The channel 4 data of the Donde Va? and WMCE satellite data set were registered to a ±1 km accuracy and made into a standard projection (Mercator). This procedure allowed accu-

Fig. 2. A satellite thermal image of the sea on July 13, 1982, in comparison with an analysis of several ships' in situ measurements of the Alboran Sea for 1967 [*Lanoix*, 1974]. The analysis indicates that the ship measurements occurred at the time of a disappearance of the eastern Alboran Gyre.

rate intercomparison of the data set and the construction of reasonable sequential loop movies of the disappearance and reestablishment of the gyres. Examples of disappearances in the western gyre are presented in Figures 3 and 4.

In Figure 3 the February 23 image shows the inflow at Gibraltar directed to the northeast and the western gyre fully formed in the Alboran Basin between 4° and 5°W. The next image, March 31, shows the inflow directed eastward, the size of the gyre substantially reduced and trapped against the Moroccan coast. The April 30 image shows the gyre reforming. In Figure 4 the June 5 image shows the inflow turning immediately to the south after exiting the strait and an almost nonexistent anticyclonic gyre. The sequence from June 5 through July 15 shows the reformation of the western anticyclonic gyre. A similar occurrence in the area of the eastern gyre is given in Figure 5, where the images show the disappearance and reformation of the eastern anticyclonic gyre. In particular, the July 7 image shows a small eastern gyre trapped against the coast east of Cape Tres Forcas and the current exiting the Alboran along the North African coast. This is a similar configuration to the wind-forced model results to be discussed below. The July 13 image shows the eastern gyre almost totally collapsed. From this image through the August 16 image, the reformation of the eastern gyre can be observed.

It should be emphasized that the changes in the dynamic events under discussion take place over a several-week period. Thus as few as two images a month can be used to tell if a gyre was or was not present. There are therefore sufficient data in the above image set to derive a preliminary history of the gyres disappearances during the period. Table 2 presents such a history and thus may be used to derive an approximation of the duration and frequency of the disappearances.

Table 2 indicates that both gyres disappeared at least once a year. Also gyres disappeared at different times, never together (this was also true for the 50 images outside of the Donde Va? and WMCE data set). It is difficult to say from Table 2 whether the disappearance of the western Alboran gyre is related to the disappearance of the eastern Alboran gyre. (As will be indicated in the model discussion below, the disappearance of either gyre appears to be unrelated to

odes
or

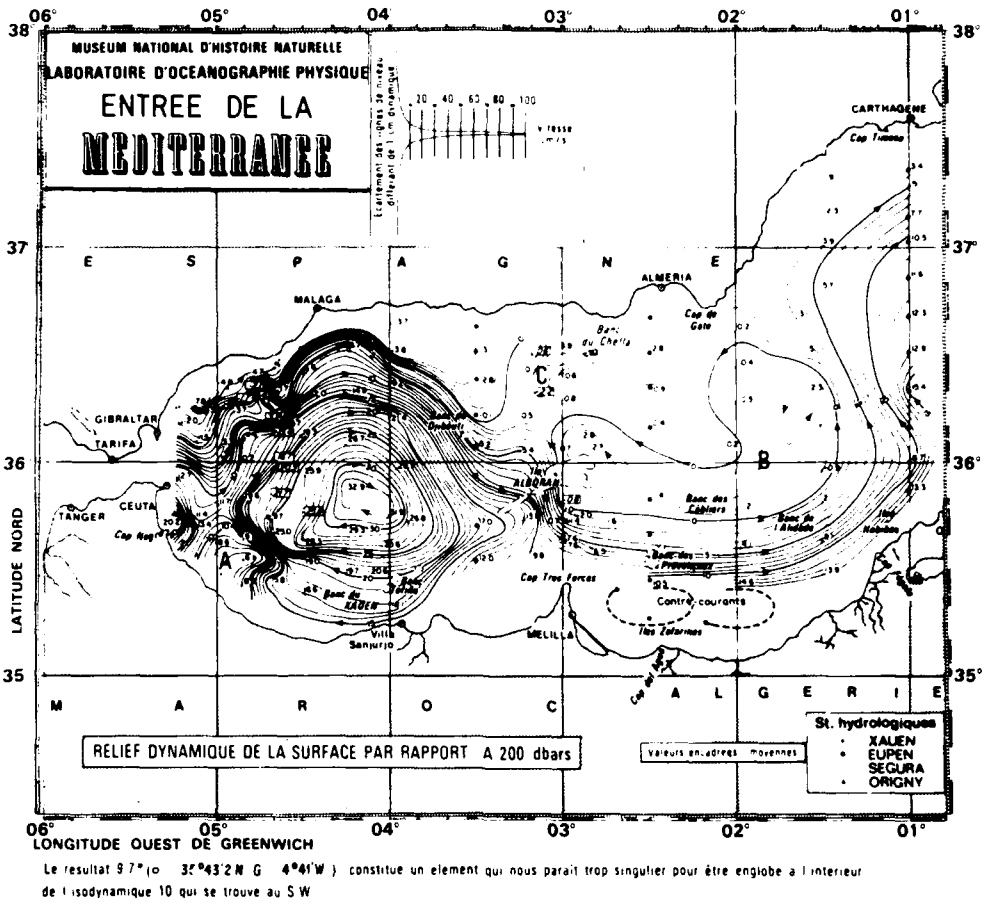

Le resultat 9 7°/o 35°43'2 N G 4°41'W) constitue un element qui nous paraît trop singulier pour être englobé à l'intérieur de l'isodynamique 10 qui se trouve au S W

Fig. 2. (continued)

the other. In fact, the model results indicate that different mechanisms may cause the disappearance of each gyre).

When either gyre disappears, it appears to do so relatively quickly. The absence of the western Alboran gyre on May 27 was not evident in imagery on May 21, 1 week earlier (Figure 6). The actual time it takes for the gyre to disappear is difficult to determine given the data distribution. Also, it is unfortunate that a daily sequence of clear sky imagery is not available to see the details of the disappearance and thus give a pictorial hint of the causal mechanism. In the disappearance of the western Alboran gyre documented by *Perkins et al.* [1990], the mooring data indicated the disappearance took place within a few days.

The return of the gyres to their fully extended positions seemed to take considerably longer. Three weeks was common, although the return of the western Alboran gyre in March 1986 took 8 weeks to recover. In their study of the western gyre disappearance of September 1982, *Perkins et al.* [1990] indicated a much shorter period: 9 days.

Numerical Ocean Circulation Model

The numerical ocean circulation models used in studying the dynamics in the western Mediterranean Sea and, in particular, the Alboran Sea are versions of a multilayer hydrodynamic thermodynamic, primitive equation model on a β plane. Various versions of the model are used to study the effects of different forcing mechanisms on the circulation dynamics of the sea. The versions used include one and two active layer, reduced gravity models, and two- and three-layer, finite depth models.

The one active layer, reduced gravity model is the simplest model which can reproduce prominent upper ocean features and is designed to simulate the first internal baroclinic mode of oceanic circulation (the term reduced gravity is derived from a balance of vertical forces in which the downward force due to the acceleration of gravity g is reduced by the upward buoyancy force, $g(\rho_2 - \rho_1/\rho)$. This model has an active upper layer (representing the inflowing

TABLE 1. Amount of Cloud-Free Images in the Alboran Sea by Month

Year	Jan.	Feb.	March	April	May	June	July	Aug.	Sept.	Oct.	Nov.	Dec.
1982	1	2	2	2	1	2	5	3	7	19	0	0
1985	0	0	0	0	0	0	0	0	0	0	1	2
1986	6	4	12	9	30	16	5	2	3	2	3	7

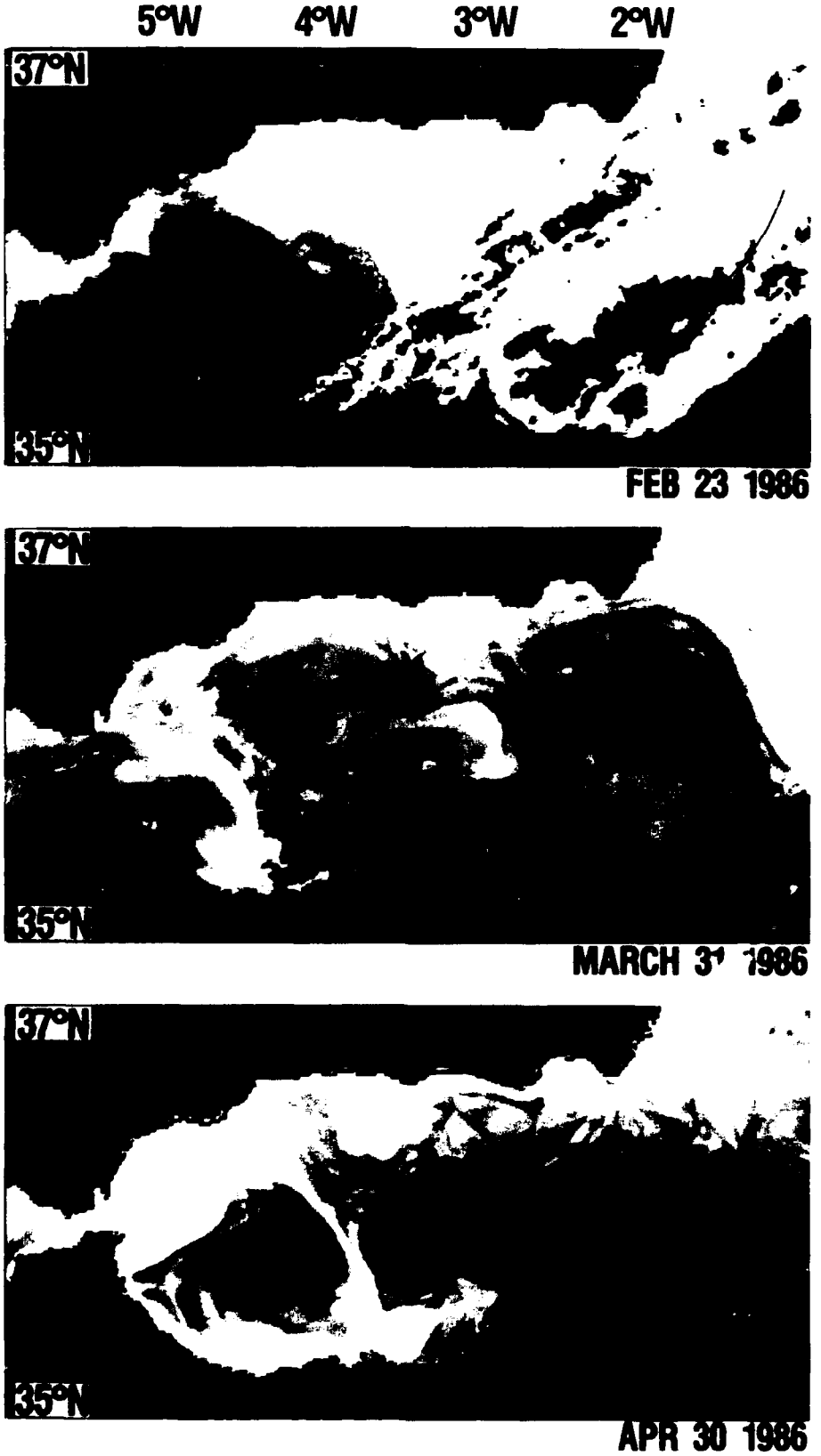

Fig. 3. Three images showing the appearance (February 23), disappearance (March 31), and reappearance (April 30) of the western Alboran gyre in early 1986. Due to lack of sufficient cloud-free imagery, it is not possible to state exactly when the disappearance occurred or when the feature reappeared.

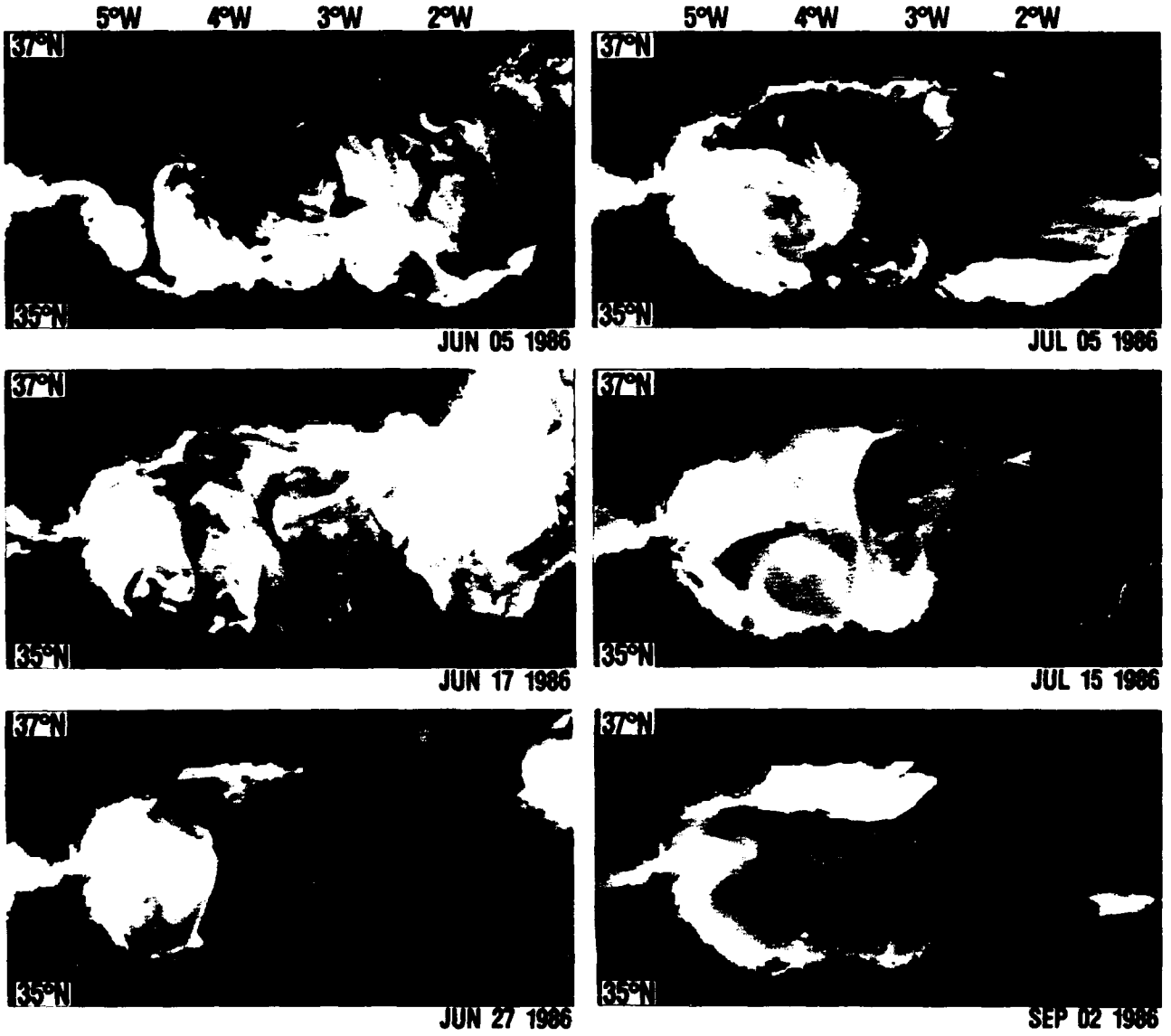

Fig. 4. A second disappearance and redevelopment of the western gyre during 1986. In this instance, more imagery are available to show the sequence of development.

MAW) separated by an impermeable interface from an infinitely deep, inert lower layer (representing the MW).

The two active layer, reduced gravity model is the simplest model which can support baroclinic instabilities and related vertical shear phenomena. This model has two active layers. The upper layer (representing MAW) is separated by impermeable interfaces from a second layer (representing LIW) and an inert, infinitely deep third layer (representing Western Mediterranean Deep Water, or WMDW). The interfaces represent the pycnoclines across which density contrasts are specified. The thermodynamic versions of the models allow interfacial (i.e., cross isopycnal) mixing and convective overturning.

The two-layer, finite depth model (with the upper layer representing MAW, and the lower layer MW) is the simplest model which includes both the effects of bottom topography, the barotropic mode, and baroclinic instabilities. The three-layer, finite depth model is the most realistic version used to date. In this version of the model, the upper layer represents MAW, the second layer LIW, and the third layer WMDW. In the finite depth versions of the model, bottom topography is confined to the bottom layer.

The governing equations for the n-layer, finite depth hydrodynamic model in the vertically integrated mass transport form in a right-handed coordinate system are

$$\frac{\partial \mathbf{V}_k}{\partial t} + (\nabla \cdot \mathbf{V}_k + \mathbf{V}_k \cdot \nabla)\mathbf{v}_k + \mathbf{k} \times f\,\mathbf{V}_k = - h_k \sum_{l=1}^{n} G_{kl} \nabla (h_l - H_l) + (\boldsymbol{\tau}_{k-1} - \boldsymbol{\tau}_k)/\rho_0 + A_H h_k \nabla^2 \mathbf{v}_k \quad (1)$$

$$\frac{\partial h_k}{\partial t} + \nabla \cdot \mathbf{V}_k = 0 \quad (2)$$

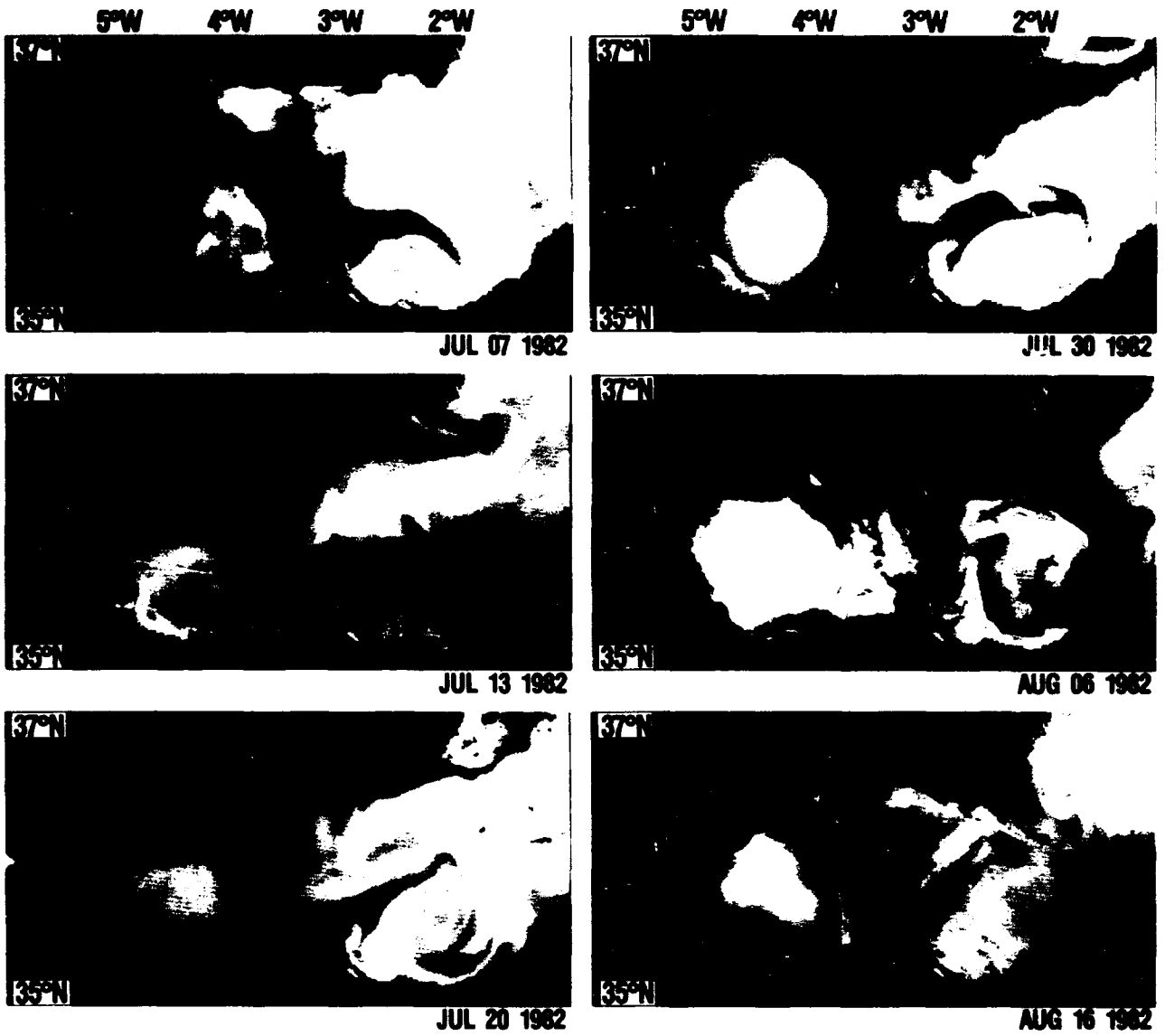

Fig. 5. The disappearance of the eastern Alboran gyre and its gradual redevelopment in 1982.

where H_k is the kth layer thickness at rest, ρ_k is the kth layer density, constant in space and time,

$$\mathbf{V}_k = h_k \mathbf{v}_k$$

$$H_n = D(x, y) - \sum_{l=1}^{n-1} H_l$$

$$G_{kl} = g \qquad l \le k$$

$$G_{kl} = g - g(\rho_l - \rho_k)/\rho_0 \qquad l > k$$

$$\tau_k = \tau_w \qquad k = 0$$

$$\tau_k = C_k \rho_0 |\mathbf{v}_k - \mathbf{v}_{k+1}|(\mathbf{v}_k - \mathbf{v}_{k+1}) \qquad k = 1, \cdots, n-1$$

$$\tau_k = C_b \rho_0 |\mathbf{v}_n| \mathbf{v}_n \qquad k = n$$

$$\nabla = \frac{\partial}{\partial x}\mathbf{i} + \frac{\partial}{\partial y}\mathbf{j}$$

where A is horizontal eddy viscosity, $f = f_0 + \beta(y - y_0)$ is the Coriolis parameter, β is differential rotation, t is time, u_k is the x-directed component of current velocity for the kth layer, v_k is the y-directed component of current velocity for the kth layer, and x, y, z are tangent plane Cartesian coordinates: x positive eastward, y positive northward, and z positive upward.

A hydrodynamic reduced gravity model with n active layers has a lowest layer that is infinitely deep and at rest, i.e., $\mathbf{V}_{n+1} = 0$, $h_{n+1} = \infty$, and $\nabla h_{n+1} = 0$. The model equations for the active layers are identical to those for an n layer hydrodynamic finite depth model, except that

$$H_n = \text{const}$$

$$G_{kl} = g(\rho_{n+1} - \rho_k)/\rho_0 \qquad l \le k$$

$$G_{kl} = g(\rho_{n+1} - \rho_l)/\rho_0 \qquad l > k$$

$$\tau_k = \tau_w \qquad k = 0$$

$$\tau_k = C_k \rho_0 |\mathbf{v}_k - \mathbf{v}_{k+1}|(\mathbf{v}_k - \mathbf{v}_{k+1}) \qquad k = 1, \cdots, n$$

TABLE 2. Presence (P) or Absence (A) of Alboran Gyre

Year	Jan.	Feb.	March	April	May	June	July	Aug.	Sept.	Oct.	Nov.	Dec.
					Western Alboran Gyre							
1982	P	A	A	A	A	P	P	P	A	P	—	—
1985	—	—	—	—	—	—	—	—	—	—	A	P
1986	P	P	A	A	P	A	A	P	P	A	A	P
					Eastern Alboran Gyre							
1982	P	P	P	P	P	A	A	A	P	P	—	—
1985	—	—	—	—	—	—	—	—	—	—	P	P
1986	P	P	P	P	P	P	P	P	P	A	P	P

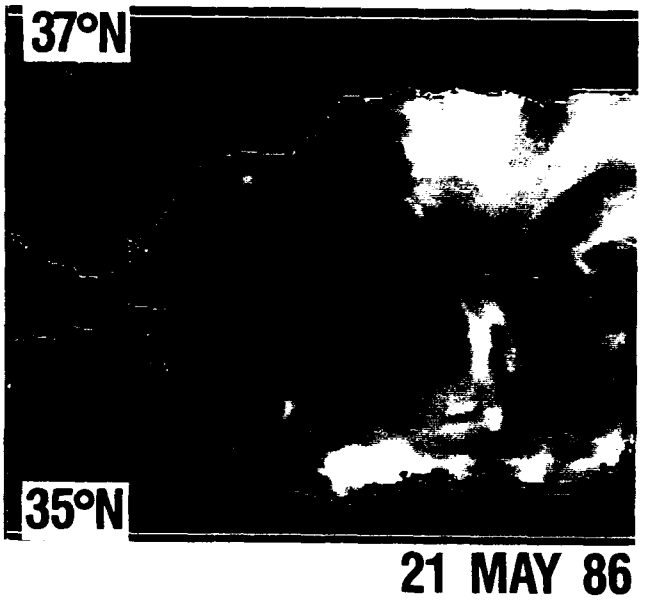

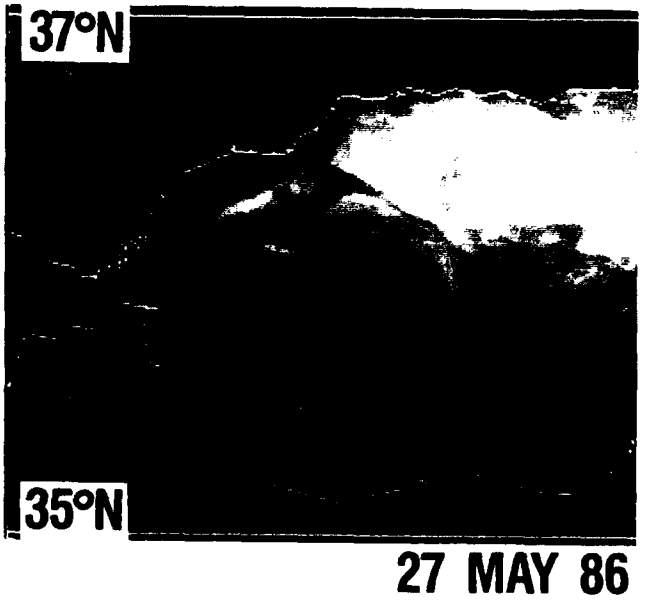

Fig. 6. An example of the rapidness of the disappearance of the western Alboran gyre. A full gyre is visible on May 21, 1986, and the first stages of the disappearance of the gyre can be seen in the image for May 27, 1986. The remaining sequence of this disappearance is shown in Figure 4.

In general, the reduced gravity model is more robust than the finite depth model, and an $n - 1$ active layer, reduced gravity model can give similar results to an n-layer finite depth model. So it is often cost effective to develop a reduced gravity model of a region first and then go on to a finite depth model.

The model equations are solved using explicit and semi-implicit versions of the *Hurlburt and Thompson* [1980] model with two important modifications: (1) the ability to handle realistic coastline geometry and (2) the addition of a modified *Orlanski* [1976] radiation outflow boundary condition at the Strait of Sicily (see *Heburn* [1987] for details). The realistic irregular model geometry (Figure 7) was created using the Synthetic Bathymetric Profiling System (SYNBAPS) [*Vanwyckhouse*, 1973, 1979] data set of bottom topography. The bottom topographic height values were interpolated from the 10-min resolution of the data set to the 0.1° longitude by 0.05° latitude (approximately 7.5 by 5 km) grid resolution of the model. The 200-m bathymetric contour was used as the physical lateral boundary of the model, and a no-slip boundary condition was applied.

Table 3 lists the parameters used in each of the model experiments in this study. Based on the in situ observations [*Lanoix*, 1974; *Katz*, 1972; *Parrilla et al.*, 1986], a mean layer depth of 200 m was chosen to represent the thickness of each of the upper two layers of the Western Mediterranean. The

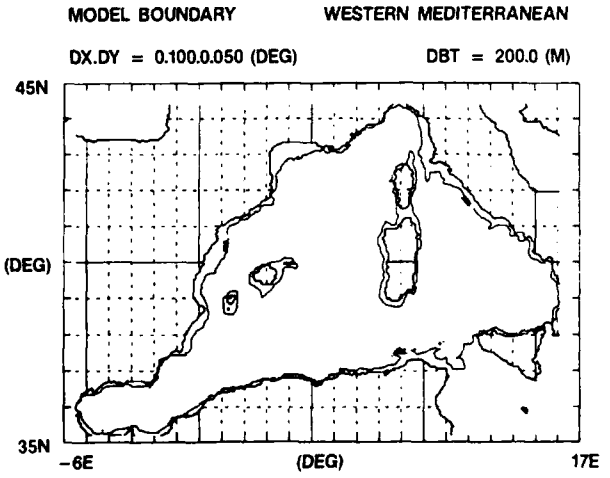

Fig. 7. Western Mediterranean model geometry. The grid spacing is 0.1° by 0.05° (~7.5 by 5 km). The model's lateral boundary is at the 200-m bathymetric contour.

TABLE 3. Model Parameters

Parameter	Definition	Value
A	eddy viscosity	100–300 m^2 s
β	(df/dy)	1.8×10^{-11} m^{-1} s^{-1}
f	Coriolis parameter	8×10^{-5} s^{-1}
g_1'	reduced gravity	0.01 m s^{-2}
H_1	undisturbed upper layer depth	200 m
H_2	undisturbed second layer depth	200 m
$\Delta x \times \Delta y$	horizontal grid resolution	0.1° × 0.05° (7.5 × 5 km)
Δt	time step	15 min
V_{1in}	inflow transport in upper layer	0, 1.6 Sv
V_{2in}	inflow transport in second layer	0, 0.6, 1.2, 1.8 Sv

nominal value for the mass flux inflow through the Strait of Gibraltar in the upper layer was taken to be 1.6 Sv with a compensating outflow through the Strait of Sicily to maintain a mass balance within the Western Mediterranean. Various observational studies [*Lanoix*, 1974; *Bethoux*, 1979; *Lacombe and Richez*, 1982; *Kinder and Parrilla*, 1984*a*, *b*] indicate mean inflows from 1.2 to 1.68 Sv and strong seasonal variations [*Bormans et al.*, 1986]. While it is recognized that the 1.6 Sv value is higher than the more recent Donde Va? estimates [*Kinder and Parrilla*, 1984*a*, *b*], its selection was made when the higher value [*Lanoix*, 1974; *Bethoux*, 1979] was the best available estimate and was retained for consistence with earlier experiments. Further experiments are planned to examine the effects of difference mean inflows and time-dependent inflow. The nominal value for the mass flux inflow through the Strait of Sicily in the second layer was taken to be 1.2 Sv [*Bethoux*, 1979] with a compensating outflow through the Strait of Gibraltar.

The climate wind-driven experiments were forced by applying monthly mean climatological wind stresses derived from 20 years (1950–1970) of ship observations in the Mediterranean [*May*, 1982]. Individual stresses were estimated from ship observations of wind speed and direction using a quadratic aerodynamic drag law with a drag coefficient dependent on the wind speed and stability. Monthly averages of the wind stresses were then calculated by averaging

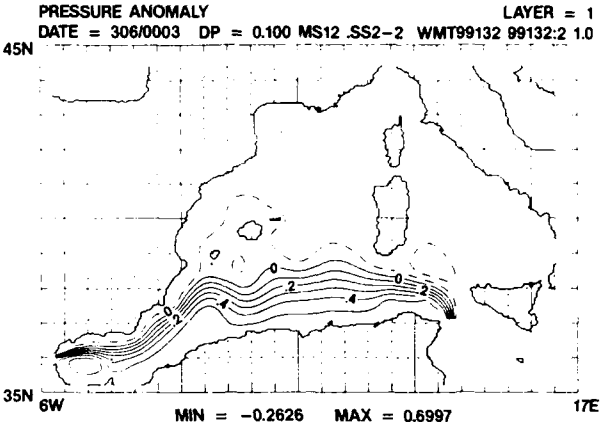

Fig. 9. Pressure deviation field for the upper layer of a two active layer, reduced gravity model experiment with inflow/outflow mass flux forcing only with zero inflow/outflow specified in the second layer. Contour interval is 0.1 m^2/s^2.

the individual wind stress estimates from each month on a 1° latitude by 1° longitude grid. These monthly averages were then bilinearly interpolated to the model grid. The climatological wind forcing is cyclic with a period of 1 year. Time-dependent wind stresses were derived from the planetary boundary layer winds from the Naval Operational Regional Atmospheric Prediction System (NORAPS), Fleet Numerical Oceanography Center's (FNOC) regional atmospheric forecast model for the Mediterranean region. The winds from the period September 1984 to August 1985 were used to examine the effects of nonclimatological winds by *Heburn* [1987].

Discussion

Although not exhaustive, numerous process studies have been conducted using the various versions of the numerical models to examine how such forcing mechanisms as mass flux inflow/outflow, wind stress, density flux, and topography may relate to the physical processes occurring in the Western Mediterranean Sea. A few of these experiments will be used to examine some of the possible underlying physical

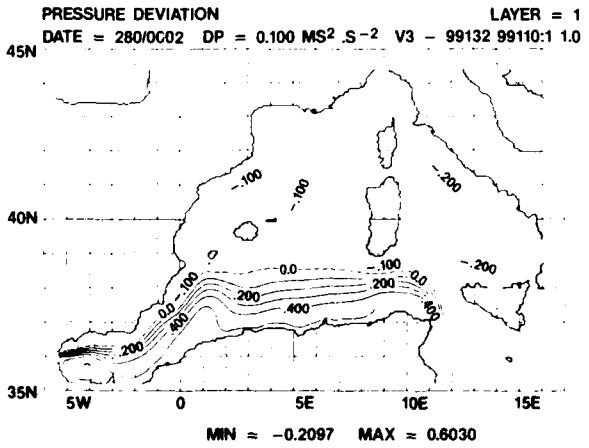

Fig. 8. Pressure deviation field for the upper layer of a one active layer, reduced gravity model experiment with inflow/outflow mass flux forcing only. Contour interval is 0.1 m^2 s^{-2}.

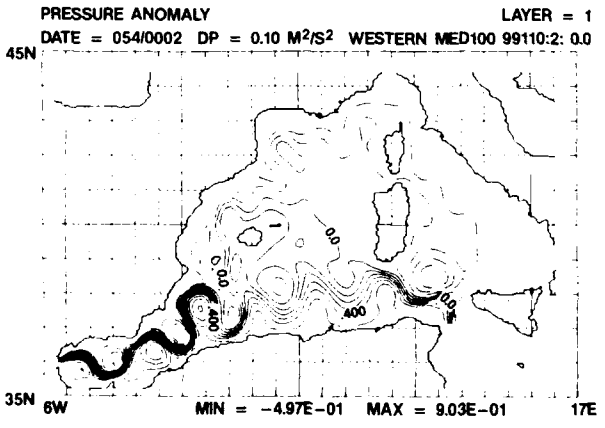

Fig. 10. Pressure deviation field for the upper layer of a two active layer, reduced gravity model experiment with inflow/outflow mass flux forcing only and 1.2-Sv inflow/outflow specified in the second layer. Contour interval is 0.1 m^2 s^{-2}.

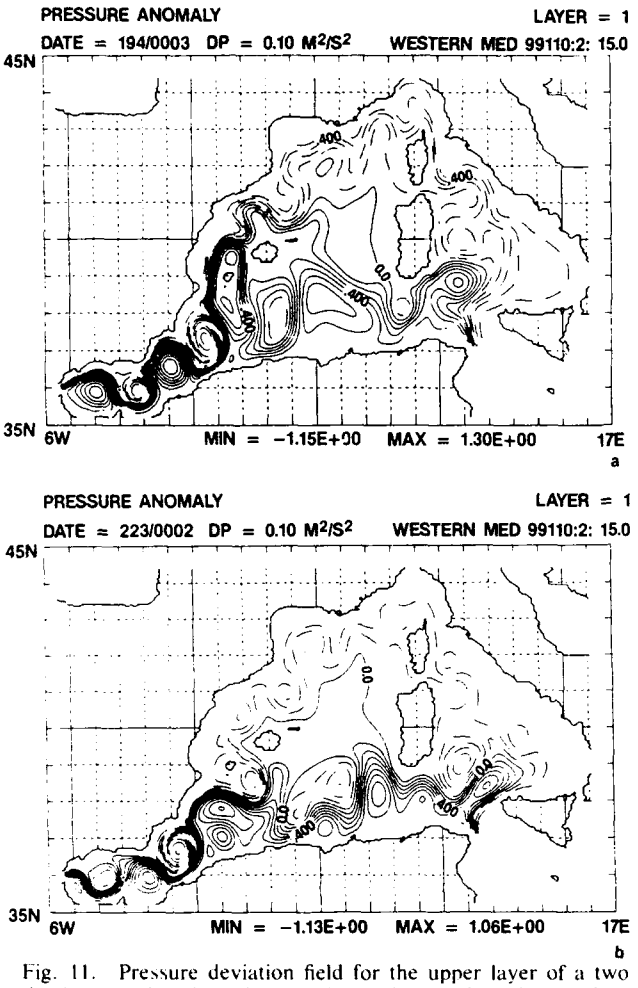

Fig. 11. Pressure deviation field for the upper layer of a two active layer, reduced gravity model experiment with inflow/outflow mass flux forcing only and 1.8-Sv inflow/outflow specified in the second layer. Contour interval is 0.1 m^2/s^2.

processes which may form the double-gyre system (e.g., Figure 1), or the single-gyre system (e.g., Figure 2).

A number of theoretical explanations have been suggested for the presence of the western anticyclonic gyre [*Nof*, 1978; *Preller and Hurlburt*, 1982; *Bryden and Stommel*, 1982; *Preller*, 1986], which indicate that the western Alboran gyre is formed and maintained primarily by the inflowing MAW. Also, these studies have shown that the basin geometry and mass flux inflow characteristics (inflow angle, vorticity profile, and vertical shear) appear to be the primary controlling factors for the location, size, and strength of the western Alboran gyre. However, these do not rule out the possibility of atmospheric variability inducing fluctuations in the gyre [*Cryson*, 1965; *Cane and Castillejo*, 1972; *Monimsen*, 1978; *Cheng and Doblar*, 1982].

Figure 8 shows the pressure deviation field for the upper layer from the one active layer, reduced gravity model. This figure illustrates the "typical" configuration for the upper layer flow when only upper layer inflow/outflow mass flux forcing is used (i.e., no winds and no inflow/outflow specified in the lower layer). What is seen is a steady state, source/sink flow with a gyre in the western basin of the Alboran and the current system exiting the Alboran along the Spanish vis-a-vis the African coast, then turning abruptly eastward through the Algerian Basin and finally exiting through the Strait of Sicily.

Preller [1986] suggests that conservation of absolute vorticity appears to be the dynamical driving mechanism for the path of the current. However, within the Alboran Basin, the constant absolute vorticity (CAV) trajectory amplitudes are restricted by the basin geometry. If the amplitudes of CAV trajectories [see *Hatliner and Martin*, 1957, pp. 353–356] were calculated based on the current velocity as it exits the Alboran Sea (approximately 35.5°N, 1.0°W), the northernmost penetration would be to 38°N. The northward penetration of the current (see Figure 8) is to 38.5°N. The southward swing of the CAV trajectories in the Algerian Basin is again influenced by the basin geometry, with the Algerian coast blocking the southward migration of the current. The alongstream velocity divergence acts to dampen the downstream fluctuations, as seen in the flow through the Algerian Basin.

While this version of the model provides insight to the basic dynamics of the formation of the western Alboran gyre, it produces a gyre which is weaker than observed. Also, it does not explain the presence of a strong eastern Alboran gyre or the preference for the double-gyre system evidenced by the satellite imagery.

A series of two active layer, reduced gravity experiments for the Western Mediterranean Sea reveal that a countercurrent in the second layer in the Alboran Basin (enhancing the vertical velocity shear and increasing the baroclinity) is vital for the formation of a strong two-gyre system [*Heburn*, 1985*b*, 1986, 1988]. In this series of experiments, the mass flux inflow through the Strait of Gibraltar in the upper layer was held constant at 1.6 Sv, while the lower layer mass flux inflow through the Strait of Sicily was specified as either 0, 0.6, 1.2, or 1.8 Sv. Figure 9 shows results from a two active layer experiment which has no mass flux inflow or outflow specified in the second layer. The upper layer results from this experiment are very similar to the one active layer results (Figure 8). Here again the results show a western Alboran gyre and the main current along the Spanish vis-a-vis the African coast as it exits the Alboran Sea.

When the mass flux inflow in the second layer through the Strait of Sicily is increased to 1.2 Sv (the nominal observed inflow), the double anticyclonic gyre system similar to that seen in the satellite imagery is observed in the model simulation (Figure 10). In this simulation the gyres in the Alboran are shown to be stationary, while the MAW, as it exits the Alboran, forming the Algerian Current, is baroclin-

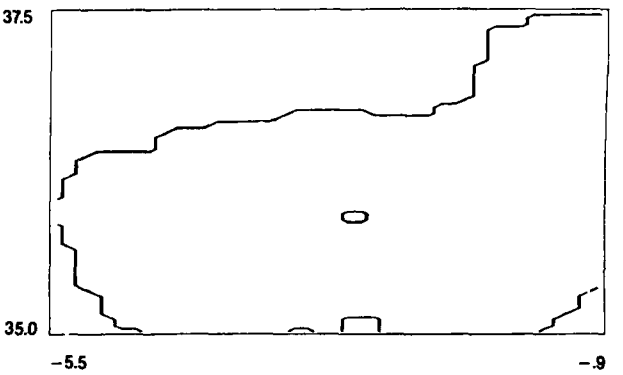

Fig. 12. Alboran Sea model geometry. Grid spacing is 10 by 5 km.

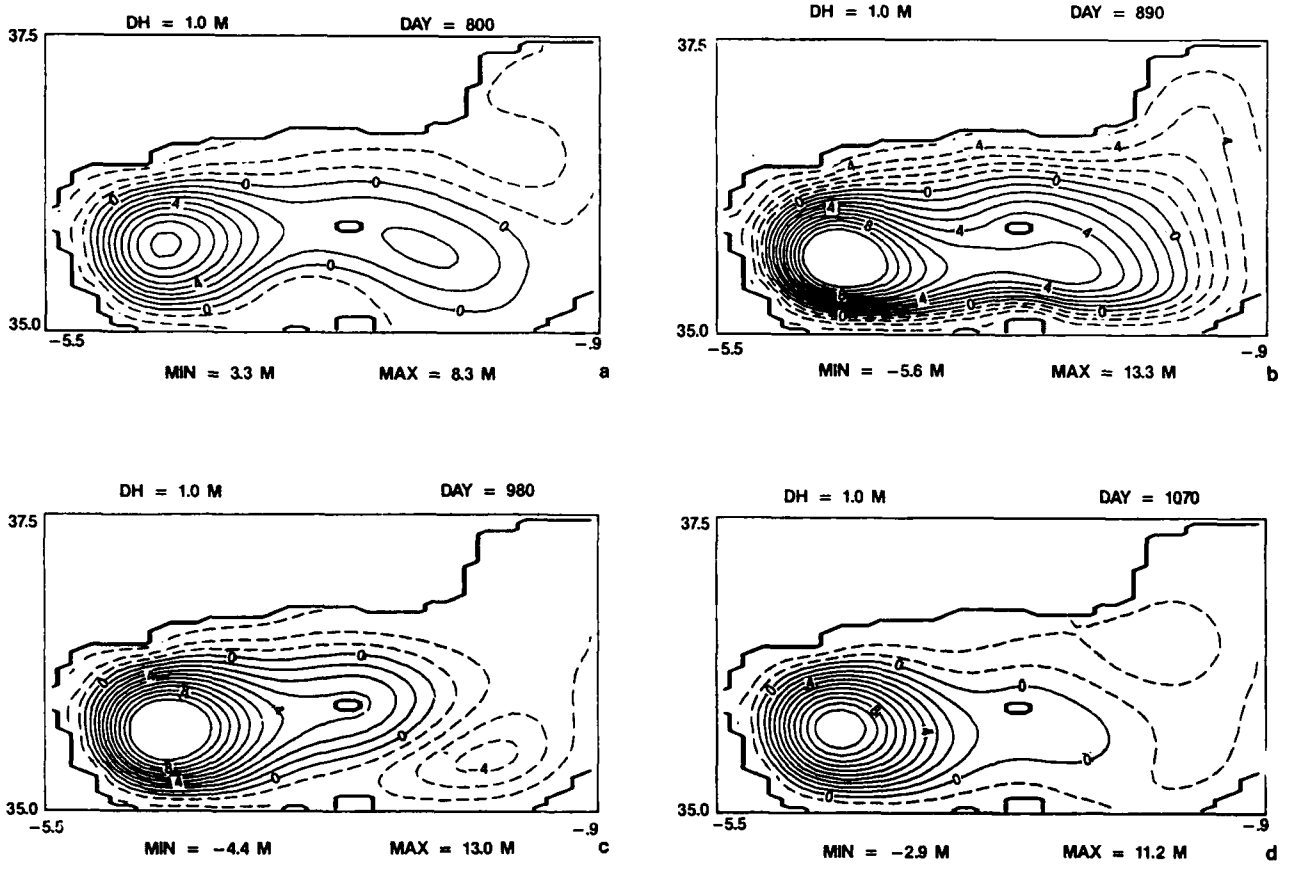

Fig. 13. Interface (pycnocline height) deviation fields from the Alboran Sea model for a one active layer, reduced gravity model experiment with climate wind forcing only. Contour interval is 1 m. (*a*) Winter, (*b*) spring, (*c*) summer, and (*d*) fall.

ically unstable, with eddy generation along the African coast, strikingly similar to the eddy generation suggested by *Millot* [1985] based on experimental results.

The formation of the double-gyre configuration results from increased anticyclonic vorticity in the upper layer at the inflow port due to increased lower layer outflow. The increase in anticyclonic vorticity causes the inflow to turn more northward [*Nof*, 1978; *Preller*, 1986] and initially to follow CAV trajectories. However, the Alboran Basin geometry prevents northward migration, forcing the flow to turn southward. The southward migration is blocked by the African coast, turning the flow back to the north. The result is the observed two-gyre system (Figure 10).

The series of two active layer, reduced gravity experiments varying the second layer inflow present some interesting results. The experiments show that as the strength of the undercurrent increases, the baroclinicity in the Algerian Basin increases with increased eddy activity, and a strengthening of the gyres and current meanders. Also, when the inflow transport in the second layer excesses that of the inflow transport of the upper layer, the meanders are observed to propagate slowly westward. Figure 11*a* is a snapshot from the case where the lower layer inflow transport through the Strait of Sicily set at 1.8 Sv and exhibits the normal two-gyre configuration. Figure 11*b* is a snapshot from this same simulation, which shows the disappearance of the western Alboran gyre and a westward displacement of the eastern Alboran gyre. This configuration is similar to that seen in the satellite images (e.g., Figure 3). In this case, the disappearance of the western Alboran gyre was due to a westward propagation of the gyres. In a steady state region, the divergence term $h_k \nabla \cdot \mathbf{v}_k$ in the continuity equation (2) is balanced by the advective term $\mathbf{v}_k \cdot \nabla h_k$, which appears to be the case in the Alboran Basin when the upper and lower layer transports are nearly equal. However, when the lower layer outflow excesses the upper layer inflow, a westward propagation occurs. *Hurlburt and Thompson* [1980] suggest that if the flow in a two-layer system can be considered to be quasi-geostrophic, then $\mathbf{v}_i \cdot \nabla h_1 \approx \mathbf{v}_{1g} \cdot \nabla h_1$ and $\mathbf{v}_{1g} \cdot \nabla h_1 = \mathbf{v}_{2g} \cdot \nabla h_1$. The magnitude of $\mathbf{v}_{2g} \cdot \nabla h_1$ is greatest when relatively strong lower layer currents flow at large angles to the gradient of the upper layer height field. This implies that upper layer height field changes can result from advection of ∇h_1 by the lower layer current $\mathbf{v}_2$.

This case (while not totally realistic in that the inflows are held constant) demonstrates one plausible mechanism for the disappearance of the western Alboran gyre, and also addresses one of the possible sources of the relative increase in transport in the lower layer. Other possible sources include enhanced transport in the lower layers due to an increased inflow transport of LIW through the Strait of Sicily, as suggested by *Manzella et al.* [1988], deep water formation within the western Mediterranean [*Bryden and Stommel*, 1982; *Sankey*, 1973; *Stommel*, 1972; *Stommel et al.*, 1973], or a decreased upper layer transport through the Strait of Gibraltar due to a number of possible physical

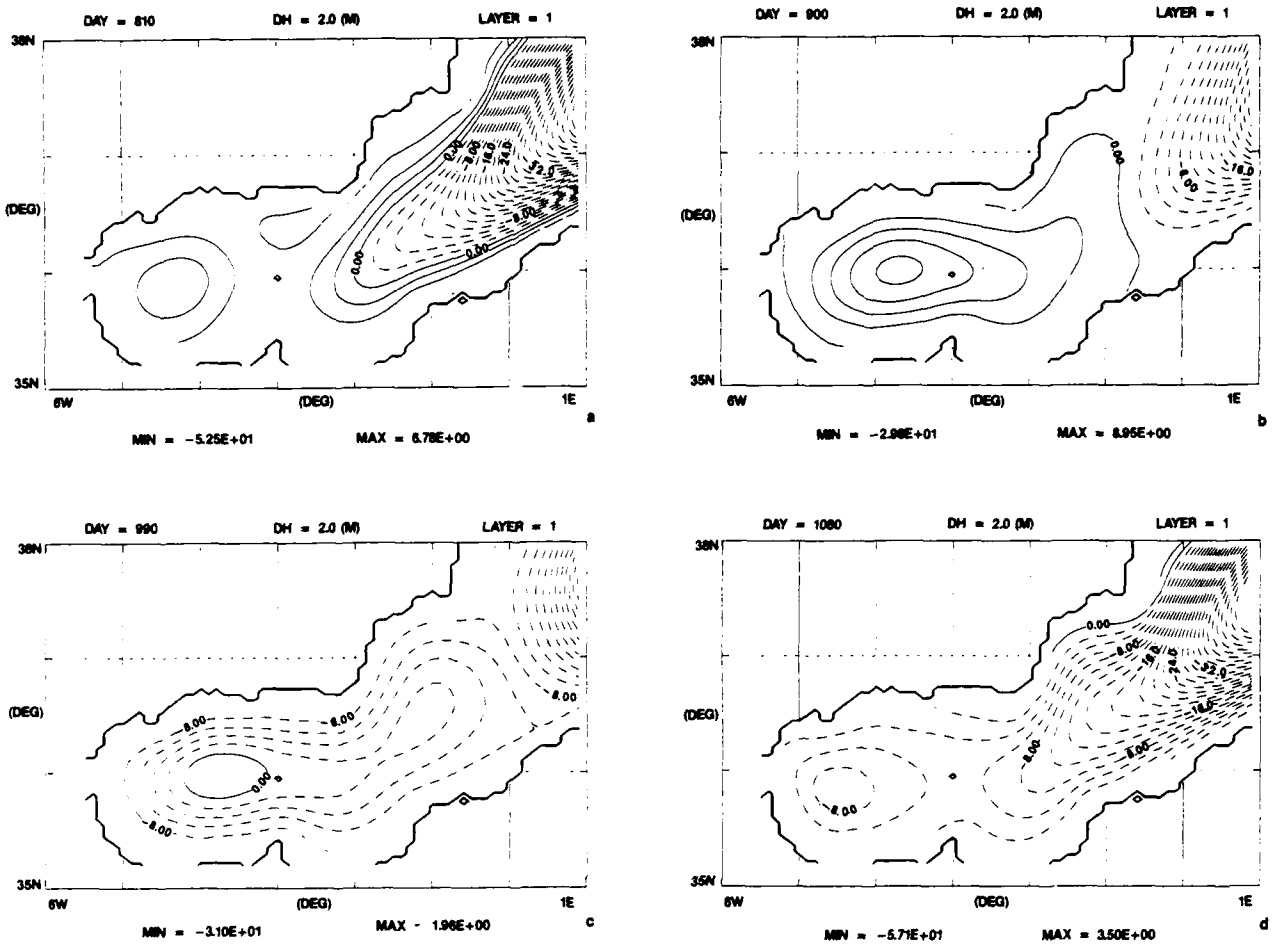

Fig. 14. Interface (pycnocline height) deviation fields from the full western Mediterranean Sea model for a one active layer, reduced gravity model experiment with climate wind forcing only. Contour interval is 2 m. (*a*) Winter, (*b*) spring, (*c*) summer, and (*d*) fall.

processes such as changes in atmospheric pressure systems, resulting in differential sea level on the Atlantic and Mediterranean sides of the Strait of Gibraltar [*Garrett*, 1983; *Bormans et al.*, 1986; *Bucca and Kinder*, 1984]. *Perkins et al.* [1990] suggest another mechanism which is related to changes in the characteristics of the inflow, specifically changes in the vorticity profile due to atmospheric effects in the Gulf of Cadiz. While the westward advection of the gyres by enhanced second-layer currents can be used to possibly explain the disappearance of the western gyre as evidenced in the two active layer, reduced gravity simulations, this forcing mechanism by itself does not replicate the single western gyre configuration seen in the satellite imagery (Figure 2). That is, the configuration with a single western gyre and a strong jet exiting the Alboran Basin along the North African coast is not seen in any of the two active layer, reduced gravity numerical simulations. Thus to simulate this flow configuration, we must include other possible forcing mechanisms, such as wind stress and, in particular, remote wind forcing. To examine the local and remote wind-generated effects on the Alboran Sea, we will use a comparison of the results from one active layer, reduced gravity models of just the Alboran Basin [*Preller*, 1986] and the entire western Mediterranean Sea. *Preller* [1986] used a model (Figure 12) of just the Alboran Sea with an open outflow boundary on the eastern side and thus could only reproduce the locally generated wind effects. However, the model used in this study (Figure 7) is of the entire western Mediterranean Sea and thus can show both the local wind effects and the remotely wind-generated effects which propagate into the Alboran Basin. Both models were forced with the same climatological wind data set [*May*, 1982] consisting of monthly means surface wind stresses on a 1° by 1° grid derived from 20 years of ship observations.

The results from the case for the Alboran Sea model, forced with annually periodic climatological winds only (Figure 13), show that the local winds generate a relatively weak western anticyclonic gyre. This gyre is strongest during spring, with a maximum interface height deviation of 13.3 m, and weakest during the winter, with a maximum interface height deviation of 8.3 m. Also, the results show that the local winds generate a seasonal response in the astern basin with an anticyclonic gyre during the winter and a cyclonic gyre during the summer in response to the periodic winds.

However, the results from the wind-only case from the full western Mediterranean model (Figure 14) present a completely different picture. In this case, the most significant influence on the circulation in the Alboran Sea comes from remotely forced, wind-generated features which propagate

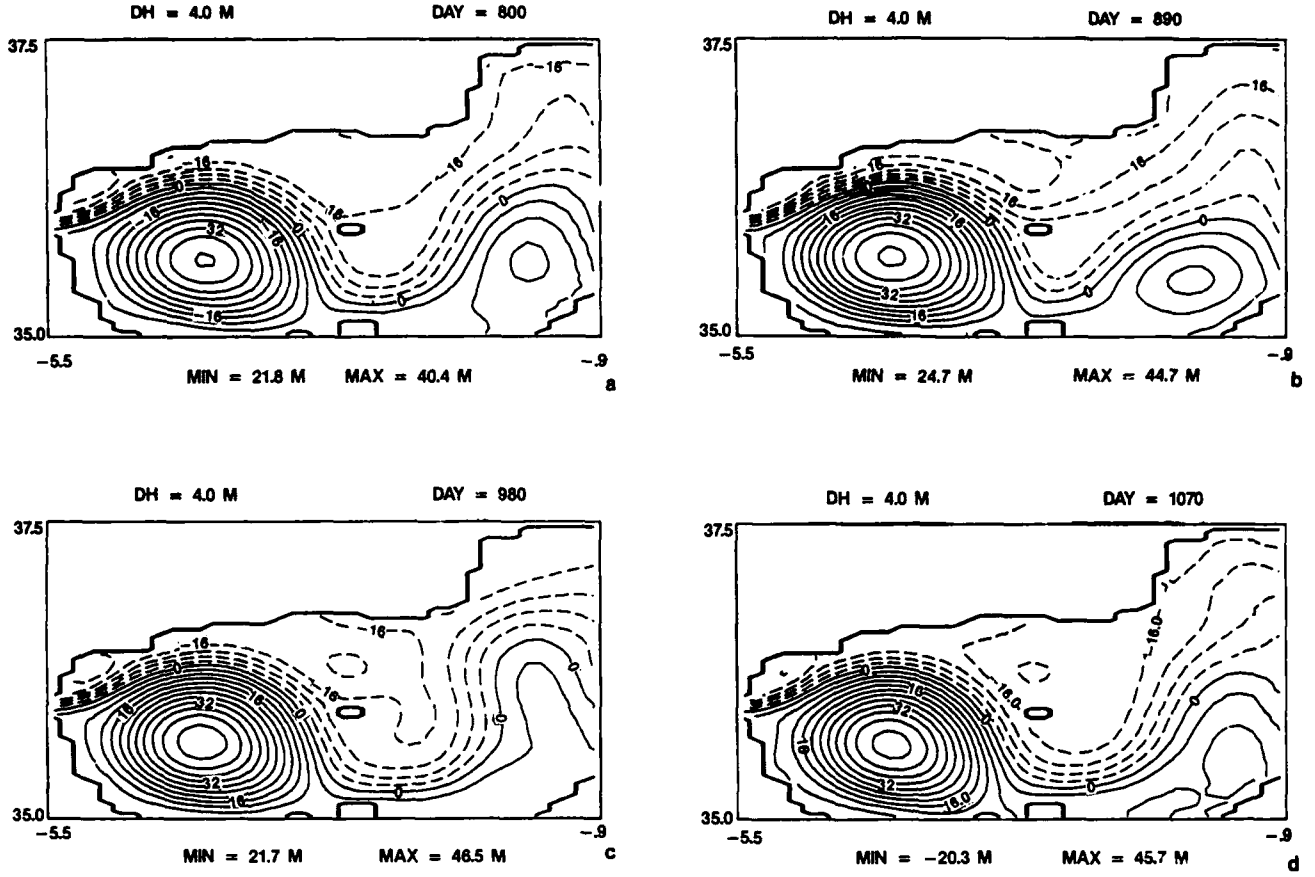

Fig. 15. Interface (pycnocline height) deviation fields from the Alboran Sea model for a one active layer, reduced gravity model experiment with both climate wind forcing and inflow/outflow mass flux forcing. Contour interval is 4 m. (*a*) Winter, (*b*) spring, (*c*) summer, and (*d*) fall.

into the Alboran Basin from the east. In the spring season the local wind effects are evident with the anticyclonic gyre appearing in the western Alboran Basin. However, during the remainder of the year, primarily during the fall and winter, the remotely forced effects dominate with a reversal of the western gyre and strong intrusion of a cyclonic circulation in the eastern part of the basin. The most striking feature of this case is the strong seasonality of the cyclonic intrusion into the eastern basin in response to the seasonally varying climatological wind stress. The large-scale cyclonic circulation is seen to invade the eastern Alboran Basin during the winter and fall, and retreat during the spring and summer. From these two cases (Figures 13 and 14), it is easy to see that remotely generated features can significantly influence the circulation in the Alboran and must be taken into account when trying to interpret the observations and to determine the causality for the observed features. Furthermore, *Heburn* [1987] showed that for the time-dependent NORAPS winds, the events in the Alboran were primarily due to effects propagating into the Alboran from the east and influencing the eastern basin more than the western basin. These cases are used to illustrate the point that remotely forced features can propagate into the Alboran Basin and modify the locally generated flow, in particular, the suppression of the eastern anticyclonic gyre. These effects must be considered when interpreting in situ and remotely sensed data. The strong seasonal signal seen in these idealized results is the result of the periodicity of the climatological wind data set used to force the model. The real winds over the Mediterranean Sea are not as nice and well behaved as the monthly mean climatological winds but are strongly episodic. Therefore it is difficult, if not impossible, to make direct comparisons between the model results and observational data, and the results presented here are only used to illustrate the processes involved. As for observation of the seasonality based on the satellite data set; there is a problem in that the satellite data set is neither sufficiently dense nor continuous to discern if a seasonal signal exists or not.

Next, the case studies with combined wind and mass flux inflow/outflow forcing will be discussed. Figure 15 presents the results from the Alboran Sea model for the combined forcing case. The results reveal that when the model is forced with both winds and inflow mass flux, the local wind effect on the circulation is minimal. It can be clearly seen that the dominate forcing mechanism for the western gyre is the inflow mass flux and that the effect of the local wind is just to slightly enhance the strength of the gyre during the summer and weaken it during the winter. The results (Figure 16) for the combined wind and inflow mass flux forced case from the full western Mediterranean Sea model show that in the Alboran Basin the inflow mass flux is the dominate forcing mechanism over all. However, the influence of the remote wind-generated features can clearly be seen in the eastern part of the Alboran Basin. As with the wind-only case, the strong wind-generated cyclonic circulation is seen to intrude into the Alboran Basin from the east during the fall

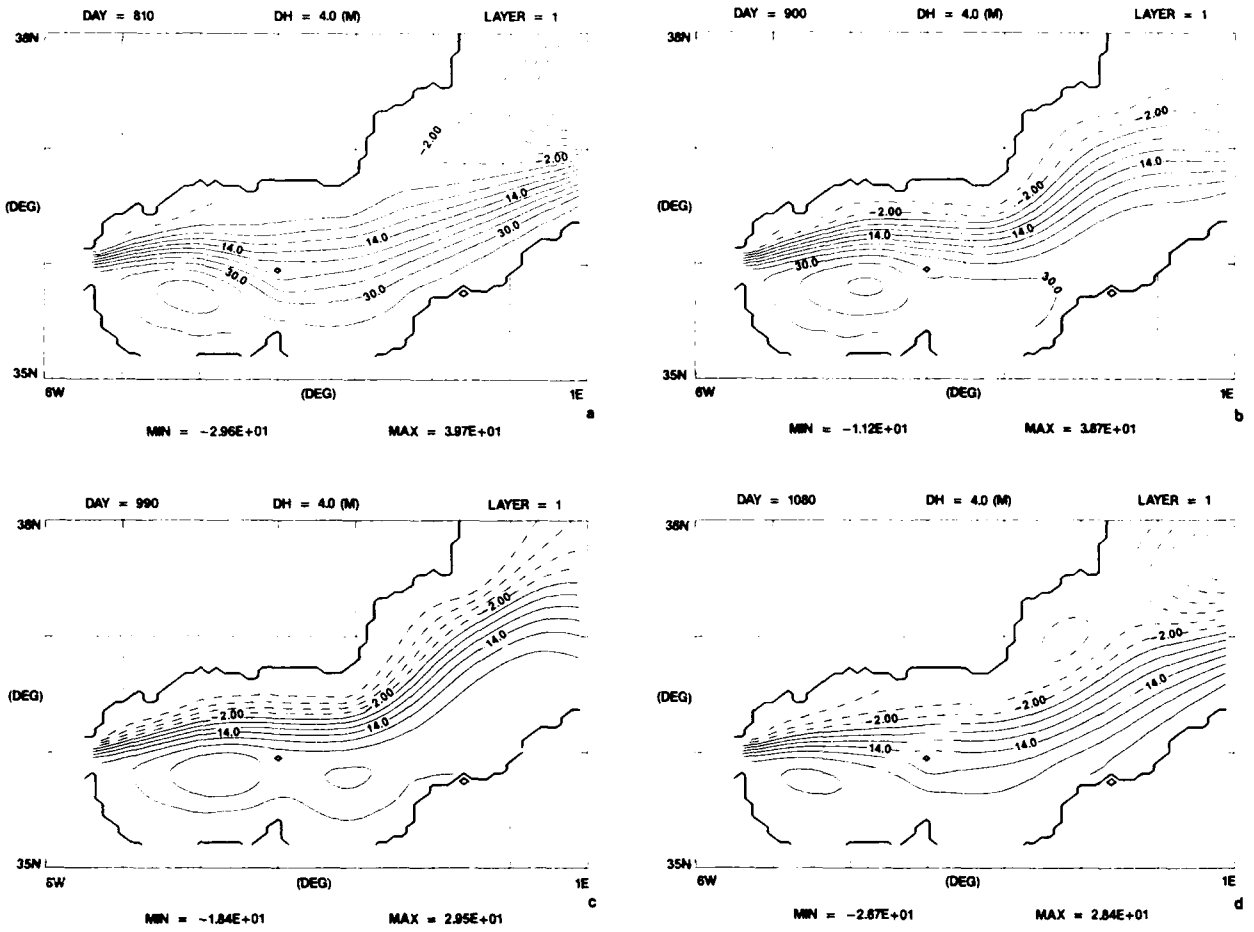

Fig. 16. Interface (pycnocline height) deviation fields from the full western Mediterranean Sea model for a one active layer, reduced gravity model experiment with both climate wind forcing and inflow/outflow mass flux forcing. Contour interval is 4 m. (*a*) Winter, (*b*) spring, (*c*) summer, and (*d*) fall.

and winter. In this case the effect of this intrusion is to suppress any anticyclonic circulations in the eastern part of the basin and to push the North African/Algerian Current close to the north African coast, a result more in line with the single-gyre configuration seen in Figure 2.

CONCLUSIONS

Considering the results of the studies discussed above, it is easy to see that the dynamics of the Alboran Sea and the entire western Mediterranean are extremely complex and that it may not be reasonable to assume that any one simple forcing mechanism (i.e., local wind stress, internal dynamics) is responsible for the observed variability. In the case of the disappearance of the western Alboran gyre, the models indicate that enhanced vertical shear between the surface layer of MAW and the second layer of LIW may be the primary forcing mechanism but do not provide a clear indication of the physical source of the enhanced shear. In the case of the eastern Alboran gyre, the models indicate that events created outside the Alboran (possibly by time-dependent winds) appear to be the chief forcing mechanism. In both cases, the models containing these forcing mechanisms came closest, of the several models and model parameters tested, to duplicating the events portrayed in the satellite imagery.

The model case studies we have presented are idealistic in that they are process studies with the inflow mass flux static, the bottom topography limited to the bottom layer, the use of climatological winds, and at rest initial states. However, even with these limitations the models do generate realistic simulations of the variations in the Alboran gyres and should therefore be seriously considered in any interpretation of the observational data, in particular when conducting dynamic studies of these features to determine the causality. A number of other model experiments are planned to examine other possible processes and the effects due to time-dependent inflow, 12 hourly, time-dependent wind forcing, deep-water formation, surface heat and salt fluxes, etc.

Acknowledgments. This work was sponsored by the Office of Naval Research, program element 61153N; the Office of Naval Technology, program element 62435N; and the Chief of Naval Operations (OP-096) via the Space and Naval Warfare System Command, program element 63207N. All the numerical model calculations were performed on the Control Data Corporation CYBER 205 at the Fleet Numerical Oceanography Center, Monterey, California. NORDA contribution JA 321:017:89. Approved for public release; distribution is unlimited.

REFERENCES

Arnone, R. A., and P. E. La Violette, Satellite definition of the bio-optical and thermal variation of the coastal eddies associated

with the African Current, *J. Geophys. Res.*, *91*(C2), 2351–2364, 1986.

Arnone, R. A., D. A. Wiesenberg, and K. D. Saunders, The origin and characteristics of the Algerian Current, *Eos Trans. AGU*, *68*(50), 1725, 1987.

Bethoux, J. P., Budgets of the Mediterranean Sea. Their dependence on the local climate and on characteristics of the Atlantic waters, *Oceanol. Acta*, *2*, 137–163, 1979.

Bethoux, J. P., Mean water fluxes across sections in the Mediterranean Sea, evaluated on the basis of water and salt budgets and of observed salinities, *Oceanol. Acta*, *3*, 79–88, 1980.

Bormans, M., C. Garrett, and K. R. Thompson, Seasonal variability of the surface inflow through the Strait of Gibraltar, *Oceanol. Acta*, *9*, 403–414, 1986.

Bryden, H. L., and H. M. Stommel, Origin of the Mediterranean outflow, *J. Mar. Res.*, *40*, Suppl., 55–71, 1982.

Bucca, P., and T. H. Kinder, An example of meteorological effects on the Alboran Sea gyre, *J. Geophys. Res.*, *89*, 751–757, 1984.

Cheney, R. E., Recent observations of the Alboran Sea, *NAVOCEANO Tech. Note 370-73-77*, 24 pp., Nav. Oceanogr. Office Stennis Space Center, Miss., 1978.

Cheney, R. E., and R. A. Doblar, Structure and variability of the Alboran Sea frontal system, *J. Geophys. Res.*, *87*, 585–594, 1982.

Donde Va? Group, Donde Va? An oceanographic experiment in the Alboran Sea, The oceanography report, *Eos Trans. AGU*, *65*(36), 682–683, 1984.

Garrett, C. J. R., Variable sea level and strait flows in the Mediterranean: A theoretical study of the response to meteorological forcing, *Oceanol. Acta*, *6*, 79–87, 1983.

Gascard, J.-C., and C. Richez, Water masses and circulation in the western Alboran Sea and in the Strait of Gibraltar, *Progr. Oceanogr.*, *15*, 157–216, 1985.

Hatliner, G. J., and F. L. Martin, *Dynamical and Physical Meteorology*, 470 pp., McGraw-Hill, New York, 1957.

Heburn, G. W., Effects of wind versus hydraulic forcing on the dynamics of the western Mediterranean Sea, *Rapp. Comm. Int. Mer Medit.*, *29*(3), 65–67, 1985*a*.

Heburn, G. W., Eddy generation along the north African coast, *Eos Trans. AGU*, *66*(51), 1324, 1985*b*.

Heburn, G. W., A numerical study of baroclinic shear instability along the north African coast, *Rapp. Comm. Int. Mer Medit.*, *30*, 165, 1986.

Heburn, G. W., The dynamics of the western Mediterranean Sea: A wind forced case study, *Ann. Geophys.*, *5B*(1), 61–74, 1987.

Heburn, G. W., A numerical study of the interaction of various forcing mechanisms on the circulation of the western Mediterranean Sea, *Rapp. Comm. Int. Mer Medit.*, *31*(2), 210, 1988.

Hurlburt, H. E., and J. D. Thompson, A numerical study of Loop Current intrusions and eddy shedding, *J. Phys. Oceanogr.*, *10*, 1611–1651, 1980.

Katz, E., The Levantine Intermediate Water between the Strait of Sicily and the Strait of Gibraltar, *Deep Sea Res.*, *19*, 507–520, 1972.

Kinder, T. H., and G. Parrilla, Hydrographic structure in the western Alboran Sea, June 1982, in *Donde Va? Meeting Report*, edited by G. Parrilla, Instituto Espanol de Oceanografía, Madrid, 1984*a*.

Kinder, T. H., and G. Parrilla, Shallow hydrographic structure in the western Alboran Sea, October 1982, in *Donde Va? Meeting Report*, edited by G. Parrilla, Instituto Espanol de Oceanografica, 1984*b*.

Lacombe, H., and C. Richez, The regime of the Strait of Gibraltar, in *Hydrodynamics of Semienclosed Seas*, edited by J. C. J. Nihoul, pp. 13–73, Elsevier, New York, 1982.

Lacombe, H., and C. Tchernia, Carateres hydrologiques et circulation des eaux en Mediterranee, in *The Mediterranean Sea*, edited by D. J. Stanley, pp. 26–36, Dowden, Hutchinson, and Ross, Stroudsberg, Pa., 1972.

Lanoix, F., Projet Alboran, Etude hydrologique et dynamique de la mer d'Alboran, *Tech. Rep. 66*, 39 pp. plus 32 figs., NATO, Brussels, 1974.

La Violette, P. E., Portion of the Western Mediterranean Circulation Experiment complete, *Eos Trans. AGU*, *68*(9), 123–124, 1987.

La Violette, P. E., T. H. Kinder, and D. W. Green III, Measurements of internal waves in the Strait of Gibraltar using a shore-based radar, *NORDA TR 118*, 13 pp., Nav. Ocean Res. and Dev. Activity, Stennis Space Center, Miss., 1986.

Manzella, G. M. R., G. P. Gasparini, and M. Astraldi, Water exchange between the eastern and western Mediterranean through the Strait of Sicily, *Deep Sea Res.*, *35*, 1021–1036, 1988.

May, P. W., Climatological flux estimates in the Mediterranean Sea, I, Winds and wind stress, *NORDA Tech. Rep. 54*, 56 pp., Nav. Ocean Res. and Dev. Activity, Stennis Space Center, Miss., 1982.

Millot, C., Some features of the Algerian Current, *J. Geophys. Res.*, *90*(C4), 7169–7176, 1985.

Nof, D., On geostrophic adjustment in sea straits and estuaries: Theory and laboratory experiments, II, Two-layer system, *J. Phys. Oceanogr.*, *8*, 861–872, 1978.

Orlanski, I., A simple boundary condition for unbounded hyperbolic flows, *J. Comput. Phys.*, *21*, 251–269, 1976.

Parrilla, G., T. H. Kinder, and R. H. Preller, Deep and intermediate Mediterranean water in the western Alboran Sea, *Deep Sea Res.*, *33*, 55–88, 1986.

Perkins, H., T. H. Kinder, and P. E. La Violette, The Atlantic inflow in the western Alboran Sea, *J. Phys. Oceanogr.*, in press, 1990.

Phillipe, M., and L. Harang, Surface temperature fronts in the Mediterranean Sea from infrared satellite imagery, in *Hydrodynamics of Semi-Enclosed Seas*, edited by J. C. J. Nihoul, pp. 91–128, Elsevier, New York, 1982.

Preller, R. H., A numerical model study of the Alboran Sea gyre, *Progr. Oceanogr.*, *16*, 113–146, 1986.

Preller, R. H., and H. E. Hurlburt, A reduced gravity numerical model of circulation in the Alboran Sea, in *Hydrodynamics of Semi-Enclosed Sea*, edited by J. C. J. Nihoul, pp. 75–89, Elsevier, New York, 1982.

Sankey, T., The formation of deep water in the northwestern Mediterranean, *Progr. in Oceanogr.*, *6*, 159–179, 1973.

Stommel, H., Deep winter-time convection in the western Mediterranean Sea, in *Studies in Physical Oceanography*, vol. 2, edited by A. L. Gordon, 232 pp., Gordon and Breach, New York, 1972.

Stommel, H., H. Bryden, and P. Mangelsdorf, Does some of the Mediterranean outflow come from great depth?, *Pure Appl. Geophys.*, *105*, 879–889, 1973.

Tintoré, J., P. E. La Violette, I. Blade, and A. Cruzado, A study of an intense density front in the eastern Alboran Sea: The Almeria-Oran Front, *J. Phys. Oceanogr.*, *18*(10), 1384–1397, 1988.

Vanwyckhouse, R. J., Synthetic Bathymetric Profiling System (SYNBAPS), *Tech. Rep. 233*, 138 pp., Nav. Oceanogr. Office, Washington, D. C., 1973.

Vanwyckhouse, R. J., SYNBAPS, volume I, Data sources and data preparation, *NORDA Tech. Note 35*, Nav. Ocean Res. and Dev. Activity, Stennis Space Center, Miss., 1979.

G. W. Heburn and P. E. La Violette, Naval Oceanographic and Atmospheric Research Laboratory, Stennis Space Center, MS 39529

(Received February 6, 1989;
revised September 11, 1989;
accepted October 25, 1989.)

REPORT DOCUMENTATION PAGE

Form Approved
OMB No. 0704-0188

1. Agency Use Only *(Leave blank).*	2. Report Date.	3. Report Type and Dates Covered.
	1990	Journal Article

4. Title and Subtitle.
Variations in the Structure of the Anticyclonic Gyres Found in the Alboran Sea

5. Funding Numbers.
Program Element No. 63207N
Project No. 0101
Task No. 100
Accession No. DN496436

6. Author(s).
George W. Heburn and Paul E. La Violette

7. Performing Organization Name(s) and Address(es).
Naval Oceanographic and Atmospheric Research Laboratory
Stennis Space Center, MS 39529-5004

8. Performing Organization Report Number.
JA 321:017:89

9. Sponsoring/Monitoring Agency Name(s) and Address(es).
Naval Oceanographic and Atmospheric Research Laboratory
Stennis Space Center, MS 39529-5004

10. Sponsoring/Monitoring Agency Report Number.
JA 321:017:89

11. Supplementary Notes.

12a. Distribution/Availability Statement.
Approved for public release; distribution is unlimited.

12b. Distribution Code.

13. Abstract *(Maximum 200 words).*

Historical satellite, aircraft, and in situ data have shown that two anticyclonic gyres (the western and eastern Alboran gyres) are major ocean features of the Alboran Sea. An examination of several years of satellite imagery indicates that large variations in the surface expression of these two gyres occur and that on occasion one or the other byre disappears (the disappearance of both gyres at the same time was not seen). The initial disappearance of either gyre occurs on a time scale of a week to 2 weeks, whereas the return may take from 3 weeks to 2 months. Various forcing mechanisms, i.e., winds, mass flux inflow through the Straits of Gibraltar and Sicily, and/or density, have been used in numerical ocean circulation models to study the dynamics of the western Mediterranean Sea. Various model results show relationships similar to those shown by the satellite imagery. However, no single forcing mechanism has been positively identified as the source of the disappearances, and the events may be a result of a combination of forcing mechanisms.

14. Subject Terms.	15. Number of Pages.
(U) Numerical Modeling; (U) Ocean Circulation; (U) Data Assimilation; (U) Nowcasting	15
	16. Price Code.

17. Security Classification of Report.	18. Security Classification of This Page.	19. Security Classification of Abstract.	20. Limitation of Abstract.
Unclassified	Unclassified	Unclassified	SAR